Published in final edited form as:
Nat Med. 2014 February ; 20(2): 209–214. doi:10.1038/nm.3436.

A technique for *in vivo* mapping of myocardial creatine kinase metabolism

Mohammad Haris[1,5], **Anup Singh**[1,5], **Kejia Cai**[1], **Feliks Kogan**[1], **Jeremy McGarvey**[2], **Catherine DeBrosse**[1], **Gerald A Zsido**[2], **Walter R T Witschey**[1,2], **Kevin Koomalsingh**[2], **James J Pilla**[2], **Julio A Chirinos**[3,4], **Victor A Ferrari**[4], **Joseph H Gorman**[2], **Hari Hariharan**[1], **Robert C Gorman**[2], and **Ravinder Reddy**[1]

[1]Center for Magnetic Resonance and Optical Imaging, Department of Radiology, University of Pennsylvania, Philadelphia, Pennsylvania, USA

[2]Gorman Cardiovascular Research Group, Department of Surgery, University of Pennsylvania, Philadelphia, Pennsylvania, USA

[3]Department of Medicine, Philadelphia Veterans Affairs Medical Center, Philadelphia, Pennsylvania, USA

[4]Department of Medicine, Cardiovascular Division, University of Pennsylvania, Philadelphia, Pennsylvania, USA

Abstract

ATP derived from the conversion of phosphocreatine to creatine by creatine kinase provides an essential chemical energy source that governs myocardial contraction. Here, we demonstrate that the exchange of amine protons from creatine with protons in bulk water can be exploited to image creatine through chemical exchange saturation transfer (CrEST) in myocardial tissue. We show that CrEST provides about two orders of magnitude higher sensitivity compared to ^{1}H magnetic resonance spectroscopy. Results of CrEST studies from *ex vivo* myocardial tissue strongly correlate with results from ^{1}H and ^{31}P magnetic resonance spectroscopy and biochemical analysis. We demonstrate the feasibility of CrEST measurement in healthy and infarcted myocardium in animal models *in vivo* on a 3-T clinical scanner. As proof of principle, we show the conversion of phosphocreatine to creatine by spatiotemporal mapping of creatine changes in the exercised

Correspondence should be addressed to R.R. (krr@mail.med.upenn.edu).
[5]These authors contributed equally to this work.

Note: Any Supplementary Information and Source Data files are available in the online version of the paper.

AUTHOR CONTRIBUTIONS

M.H. and A.S. designed and performed experiments, analyzed data and wrote the manuscript; K.C. provided technical support with animal studies and helped with manuscript editing; F.K. performed experiments and helped with human subject scanning and manuscript editing; J.M. helped with animal handling and manuscript editing; C.D. helped with human subject scanning; G.A.Z. helped with animal handling and scanning; W.R.T.W. provided technical support with animal imaging; and K.K. and J.J.P. helped with animal handling and preparation for imaging. J.A.C., V.A.F. and J.H.G. advised on cardiovascular imaging aspects and contributed to manuscript editing; H.H. provided pulse sequence design and technical guidance and contributed to the manuscript writing; R.C.G. helped with animal experimental design and contributed to manuscript editing; and R.R. conceived of and designed the study and contributed to manuscript writing and editing.

COMPETING FINANCIAL INTERESTS

The authors declare no competing financial interests.

human calf muscle. We also discuss the potential utility of CrEST in studying myocardial disorders.

Developments over the past two decades have established a variety of magnetic resonance imaging (MRI) techniques as powerful noninvasive tools for investigation of cardiac dynamics, function and morphology[1–5]. Delayed gadolinium-enhanced MRI provides an adequate assessment of myocardial viability[6]. Nuclear imaging techniques have also been used earlier in assessment of myocardium tissue viability, including detection of glucose metabolism with ^{18}F-fluorodeoxyglucose[7], assessment of cell membrane integrity with thallium-201 (refs. 8–10) and identification of intact mitochondria with technetium-99m sestamibi[10,11].

The creatine kinase (CK) reaction has a vital role in myocardial energetics. ATP derived from the conversion of phosphocreatine (PCr) and ADP to creatine (Cr) by CK provides an essential chemical energy source that governs myocardial contraction. Whereas ATP represents the body's fundamental energy currency, PCr serves as the reservoir of cellular energy. During ischemia, PCr is depleted to maintain ATP supply. Previous studies have shown that persistent ischemia produced by coronary occlusion depletes all of the PCr and eventually the ATP supply, leading to myocardial infarction[12,13]. Further studies have shown that in patients with heart failure, cardiomyopathy and diabetes, Cr, PCr and ATP concentrations are reduced in myocardium, which potentially links energy deprivation with contractile dysfunction in the failing heart[14–18]. Thus, measurement of metabolites involved in the tissue CK reaction serves as a way to investigate the role of energy deprivation in the failing heart and to assess local ischemia and cardiomyocyte oxygenation, remodeling and viability.

Currently, ^{31}P and ^{1}H magnetic resonance spectroscopy (MRS) are the standard methods for measuring CK metabolites *in vivo*[14–17,19,20]. ^{31}P MRS enables measurement of PCr, ATP and their ratios, as well as CK kinetics[15,16,19,20]. ^{1}H MRS, on the other hand, measures total Cr composed of free Cr and PCr[14,17]. However, in general, MRS techniques are limited by low spatial resolution and long acquisition times and are not adequate to map the heterogeneous distribution of these metabolites in various myocardial segments.

MRI based on chemical exchange saturation transfer (CEST) has been widely used to map different metabolites and macromolecules *in vivo*[21–26]. We have previously described a noninvasive, nonradio-active and high-resolution MRI technique for imaging Cr (CrEST) with solutions of CK metabolites and *ex vivo* tissue experiments (A.S., M.H., K.C., H.H. and R.R., unpublished data). This method exploits the CEST effect of Cr amine (NH_2) protons with those of bulk water. There have been no known *ex vivo* or *in vivo* studies of this method in myocardial tissue.

In this study, we demonstrate the enhanced sensitivity of CrEST over ^{1}H MRS in *ex vivo* noninfarcted myocardial tissue in a whole-body 3-T scanner. Next, we validate the dominant contribution of Cr to the CrEST effect in *ex vivo* myocardial tissue using ^{1}H and ^{31}P MRS. Finally, we show the feasibility of mapping the Cr signal *in vivo* from healthy as well as infarcted myocardium in an animal model. As proof of principle, we demonstrate the

conversion of PCr to Cr by spatiotemporal mapping of Cr changes in the human calf muscle before and after exercise. We discuss the potential overlap of Cr signals from other major metabolites of myocardium as well as the advantages and limitations of this approach.

RESULTS

Ex vivo myocardial tissue spectroscopy and imaging

Non–water-suppressed high-resolution ^{1}H MRS shows the resonance of labile NH_2 protons at ~1.8 p.p.m. downfield from water (~6.5 p.p.m., with respect to tetramethylsilane) both in 100 mM Cr solution in PBS[27] (Fig. 1a) (reproduced from ref. 27 with permission from John Wiley and Sons) and excised lamb *ex vivo* heart tissue (Fig. 1b), which broadened with increase in temperature. Unless otherwise specified, we report all frequency offsets in this work with respect to water. In the *ex vivo* myocardium, as PCr, ATP and ADP concentrations are expected to be negligible, the observed amine resonance is presumably from Cr. This is consistent with the literature reports on the skeletal muscle[28]. The anatomical image and corresponding gray and color CrEST maps from noninfarcted lamb *ex vivo* myocardial tissue are shown (Fig. 1c–e). CrEST maps showed homogeneous distribution of CrEST contrast. We observed a mean of ~10.5% CrEST contrast for the region of interest (ROI) (Fig. 1c). In measuring Cr content, CrEST provided >70-fold higher sensitivity compared to the typical ^{1}H MRS method (Fig. 1f,g). The higher sensitivity of this method can be exploited to map the Cr content at high spatial resolution in myocardium. We measured the total Cr concentration from the ROI as ~13.3 mM (Fig. 1h). With a saturation pulse length of 250 ms, we found that a saturation pulse amplitude (root mean square B_1 (B_{1rms})) of 155 Hz (3.6 μT) gave an optimal CrEST effect from *ex vivo* myocardium (Fig. 1i,j).

Cr changes in *ex vivo* lamb heart tissue imaged at two time points after excision exhibited a gradual reduction in CrEST contrast with a corresponding reduction in Cr concentration measured via ^{1}H MRS (Fig. 2a–f). The mean sensitivity (n = 26) of CrEST is 0.8% CrEST contrast per 1 mM of Cr in *ex vivo* myocardium at 37 °C (Fig. 2g), with experimental parameters as described in Online Methods. An intercept of 0.4% seems to be due to contamination from other metabolites and macromolecules present in myocardial tissue. We also measured Cr concentration in *ex vivo* myocardial tissue using biochemical analysis through the perchloric acid (PCA) extraction method[29,30]. The PCA-measured Cr concentration also correlated well with CrEST contrast, with a slope of 0.8% CrEST contrast per mM of Cr (Fig. 2h). We observed a positive correlation (r^2 = 0.92) between PCA-measured Cr and ^{1}H MRS–derived Cr concentrations, with a slope of 1 mM (PCA-measured Cr per 1 mM of ^{1}H MRS–derived Cr) (Fig. 2i).^{31}P MRS from the *ex vivo* noninfarcted myocardial tissue showed only resonance from inorganic phosphate (P_i) and no signals from PCr or ATP (Fig. 2j), which implies that the observed CrEST contrast and the Cr concentration derived from^{1}H MRS from myocardial tissue are predominantly from free Cr.

CrEST maps from swine *ex vivo* myocardial tissue demonstrate lower CrEST contrast in the infarcted region (Fig. 3a–c). The CrEST contrast (mean ± s.d.) in infarcted and normal regions was 4.7 ± 1.2% and 10.4 ± 2.0%, respectively (Fig. 3b,c). These CrEST contrast values are consistent with those obtained from Cr concentration values measured from

biochemical analysis and spectroscopy[31]. Trichrome staining of the same tissue showed clear demarcation of the infarcted area as blue and the noninfarcted area as red (Fig. 3d). Data from another swine *ex vivo* myocardial tissue is also shown (Fig. 3e–i). The CrEST contrasts for the voxels placed on the anatomic image (Fig. 3f) were 3.8% and 10.8%, respectively, in infarcted and noninfarcted regions. For the same voxels, ^{1}H MRS showed a corresponding change in the Cr concentration (4.3 mM in infarcted region and 13.5 mM in noninfarcted region, Fig. 3i).

In vivo myocardial imaging

We present the anatomical images and grayscale and color-coded CrEST maps from two healthy swine (Fig. 4a,b), two sheep with myocardial infarct (imaged 1 week after infarction, Fig. 4c,d) and one swine with a myocardial infarct (imaged 8 weeks after infarction, Fig. 4e). The grayscale and color-coded CrEST maps from two healthy swine show rather uniform CrEST contrast in myocardium (Fig. 4a,b). In all infarcted swine and sheep, the CrEST contrast from the normal myocardial regions was higher than that from the infarcted regions (Fig. 4c–e). The *Z* spectra from infarcted regions are narrower than those from the normal regions. A typical example is shown in Figure 4f. The consistency of CrEST contrast values in normal and infarcted regions in all animals studied is depicted in a bar graph (Fig. 4g). A delayed gadolinium-enhanced image from one of the swine myocardium 8 weeks after infarction depicts hyperenhancement in the infarcted myocardial region, indicating the presence of the contrast agent (Fig. 4h). The CrEST maps of the same slice show decreased CrEST contrast in the infarcted region compared to the noninfarcted region (Fig. 4e). In sheep imaged 1 week after infarction (Fig. 4c,d), the CrEST contrast in infarcted myocardium tissue was slightly higher than that in the swine imaged 8 weeks after infarction (Fig. 4e). This could be owing to the progressive decrease in Cr concentration over the period of 8 weeks. The skeletal muscles from the chest region also exhibit CrEST, but this does not interfere with the CrEST from the myocardium (Fig. 4a–e).

Imaging of exercise-induced Cr changes in human calf muscles

We further validated the CrEST method *in vivo* by changing the Cr concentration in human calf muscles ($n = 3$) through in-magnet plantar flexion exercise. Immediately after exercise, we observed increased CrEST contrast, which then recovered to basal value (Fig. 5a). The average CrEST contrast in the soleus and medial gastrocnemius muscles at baseline and following exercise is plotted as function of time (Fig. 5b). Following exercise, we observed an initial increase in CrEST contrast of 2.2% in the soleus muscle and 3% in the medial gastrocnemius muscle over baseline values. These changes were validated with changes in PCr measured with ^{31}P MRS. ^{31}P MRS showed decreased PCr and increased P_i after exercise, and both recovered to the basal value in due course (Fig. 5c). The time course of PCr measured from ^{31}P MRS shows a decrease following exercise, which exponentially recovers back to baseline values (Fig. 5d). There was no change in pH as measured from the ^{31}P MRS. In these experiments, we did not observe any measurable changes in either water T_2 relaxation time or in magnetization transfer ratio (MTR) (data not shown). We observed similar results in all three healthy subjects studied (data not shown).

DISCUSSION

Previously, we have shown that solutions of PCr, ADP and ATP at their physiological concentrations showed no significant contribution to CrEST contrast, whereas the CrEST contrast from the Cr solution was linearly proportional to the Cr concentration in the physiological concentration range[27]. The very slow exchange rate of amine protons on PCr, ADP and ATP compared to that of amine protons on Cr, as well as the difference in the chemical shift of their amine resonances and the unfavorable experimental parameters, might be the primary reason for their negligible contribution to CrEST.

Owing to the relatively short T_2 in tissue, there will be a considerable direct water saturation effect that somewhat diminishes sensitivity of the CrEST measurement. Although normalization with the image obtained with saturation at negative offset frequency (S_{-ve}) would alleviate this problem to some extent[32], the resulting CrEST effect cannot be compared directly with that from solutions. Hence, the calibration of CrEST magnitude with ^{1}H MRS was made on *ex vivo* tissue under physiological conditions. These results show that under physiological conditions, the CrEST effect is estimated to be about two orders of magnitude more sensitive than ^{1}H MRS.

Literature reports from ^{1}H MRS and ^{31}P MRS data suggest that *in vivo* myocardial tissue has a free creatine concentration of ~13.6 ± 6.7 mM (mean ± s.d.) and a PCr concentration of ~10.3 ± 2.1 mM (mean ± s.d.)[31]. *In vivo* healthy myocardial tissue exhibits a maximum of ~11.7 ± 2.3% (mean ± s.d.) CrEST contrast, which is consistent with the expected free Cr concentration and the observed ~0.8% CrEST contrast per 1 mM Cr from our *ex vivo* tissue data. The CrEST contrast measured from infarcted tissue (6.4 ± 2.6%, mean ± s.d.) is also consistent with the reported Cr concentration from infarcted tissue[33].

In this study, owing to the respiratory and cardiac gating of the acquisition, the scan time of the entire CrEST scan is ~45 min. The lengthy scan time precludes us from computing the conversion of PCr to Cr in the heart that occurs on a time scale of about 1 min. Therefore, as the same CK reaction is operative in the skeletal muscle, we have demonstrated the PCr conversion to Cr before and after mild plantar flexion exercise of human calf muscle in the magnet. Mild exercise produced a substantial increase in CrEST contrast immediately after exercise that correlated with the PCr depletion measured via ^{31}P MRS. Assuming the baseline concentration of ~10 mM for Cr and ~33 mM for PCr, the relative changes in CrEST contrast- and ^{31}P MRS–acquired PCr integrals are consistent with a conversion of ~5 mM PCr into Cr. It should be noted that the magnitude of CrEST in the calf muscle is lower than that from myocardium owing to the shorter T_2 of skeletal muscle and estimated lower Cr concentration[34,35].

These preliminary *in vivo* results, along with the association between PCr decrease and CrEST increase in the human calf muscle study, indicate that the predominant contribution to CrEST is from free Cr and that contribution from PCr, ADP and ATP is negligible. The intercept observed in the correlation plot indicates that there is a small contribution from amine groups from other metabolites or macromolecules. Our data show the feasibility of

computing CrEST maps from both normal and ischemic myocardium of swine and sheep *in vivo*.

In *in vivo* hearts studied here, in addition to myocardial CrEST, some blood signal was visible in the left ventricle. This is owing to the fact that there was some variability in heart rates of animals during the course of the experiment. As a result, a part of the acquisition time falls in the systolic phase, which causes the contrast from moving blood to be visible in the images, potentially owing to the intrinsic CEST effect from blood. This may be mitigated to a large extent by employing blood suppression techniques.

With further optimization of the imaging acquisition schemes by employing keyhole imaging[36] or k-space–weighted image contrast[37] approaches and with the inherently slower heart rates in humans compared to animals observed in this study, it is feasible to reduce the human cardiac CrEST scan time substantially. This potentially enables detecting conversion of PCr to Cr in *in vivo* myocardium. If successful, in addition to detecting ischemia, this technique will have an impact on assessing the potential inchoate metabolic derangements in the myocardium.

Static magnetic field (B_0) inhomogeneity could interfere with the selective saturation frequency and make the two selective frequencies asymmetric to bulk water. In that case, the CEST effect would reflect differences between direct saturation and magnetization transfer effects and yield a spurious CEST effect. However, the *Z*-spectrum fitting approach employed in this work mitigates these effects. The CEST effect is also highly dependent on the saturation pulse amplitude. With fixed saturation duration, a higher B_1 often induces a higher CEST effect. At 3-T field strength and with the experimental parameters used here, B_1 inhomogeneity effects are not significant and can be further mitigated by localized transmitter calibration.

The potential contribution of MTR asymmetry to CrEST contrast, due to the bound pool of water from rigid macromolecules in biological tissues, cannot be excluded in CrEST measurements based on conventional asymmetry analysis. The fitting approach used here is not significantly affected by MTR asymmetry. MTR effect, if any, potentially competes with the CrEST and would lead to an underestimation of actual CrEST levels. In the ischemic and infarcted regions of myocardium, changes in T_2, MTR and water content are expected to introduce changes in CrEST. Whereas an increase in water content leads to a reduction in Cr concentration and hence CrEST, a decrease in MTR and an increase in water T_2 lead to increased CrEST owing to reduced direct water saturation. Thus, the effects of changes in water content, MTR and T_2 compete with each other, and thereby their net effect on CrEST may not be appreciable. The strong correlation between the measured and the reported myocardial Cr concentrations and CrEST results presented in this study, from both healthy and ischemic myocardial tissue, indicates that the contributions from MTR and T_2 effects to CrEST contrast are rather small.

Another factor that may affect CrEST contrast is pH. Our previously mentioned unpublished preliminary results show that with a ± 0.5 unit change from a neutral pH of 7.0, CrEST is reduced by 1–2%. Because the infarcted region of myocardium is expected to have a pH

between 6.5 and 7.0, the CrEST contrast from these regions would be somewhat underestimated. Consequently, the lower CrEST contrast observed in the infarcted myocardium may be the result of an integrated effect of both lower pH and lower Cr concentration compared to those in healthy tissue. Thus, although pH may influence the magnitude of CrEST, it would only enhance the capability of CrEST in discriminating between healthy and infarcted myocardium.

Compared to hyperpolarized ^{13}C MRI[38], CrEST has several advantages. Unlike ^{13}C MRI, CrEST does not require any exogenous contrast agent, it is based on ^{1}H MRI and it can be readily implemented on a clinical scanner. Further comparison of these methods is included in the Supplementary Discussion.

For proof-of-principle purposes, in the current study, we imaged only a single slice with a two-dimensional imaging sequence. However, by using keyhole imaging methods or k-space–weighted image contrast approaches, it is feasible to implement a three-dimensional acquisition of CrEST maps with reasonable scan time.

The technique presented herein, if successfully applied in humans, holds potential for clinical applications without administration of any exogenous contrast agent. The assessment of myocardial viability is useful for clinical decision-making in patients with coronary artery disease. In addition, CrEST mapping may reveal the size of the border zone, although this remains to be proven.

The potential clinical applications of CrEST imaging go well beyond myocardial viability. Previous ^{31}P MRS studies from the anterior wall of the left ventricle of healthy human subjects have shown substantial reductions in PCr (~20%) after stress induced by atropine-dobutamine[39]. As CrEST detects free Cr concentration in the tissue, we hypothesize that it can detect stress-induced ischemia and the presence of coronary artery disease. As stated above, further work is required to test this hypothesis. Finally, CrEST imaging may be useful in phenotyping failing nonischemic myocardium of various etiologies, assessing the metabolic state of the myocardium and guiding therapy optimization.

In summary, this preliminary study suggests that noninvasive, non-radioactive and high-spatial-resolution mapping of free Cr in myocardial tissue is feasible *in vivo* using the CrEST technique. CrEST does not require any exogenous contrast agent, provides about two orders of magnitude higher sensitivity compared to ^{1}H MRS, can be readily implemented on 3-T clinical MRI scanners and is expected to contribute to the early diagnosis of myocardial disorders.

ONLINE METHODS

Magnetic resonance spectroscopy at 9.4 T

We performed non–water-suppressed high-resolution ^{1}H NMR spectroscopy from 100 mM Cr solution in PBS and *ex vivo* normal lamb tissue on a 9.4-T (VARIAN) scanner using a 5-mm probe at two different temperatures (25 °C and 37 °C) with singlepulse– acquired spectroscopy (TR, 4 s; number of averages, 128). From the same *ex vivo* tissue, we

performed ^{31}P MRS at 9.4 T using a pulse-acquired sequence (TR, 4 s; number of averages, 128).

Magnetic resonance imaging and magnetic resonance spectroscopy at 3 T in *ex vivo* tissue

Normal lamb left ventricular myocardial tissue samples (n = 20) from a local butcher shop (killed within 18 h) and swine heart tissue samples (n = 6) with left ventricular myocardial infarction after terminal experiments were obtained and kept in the PBS (pH 7.0). All the swine tissue sample experiments were performed under a protocol approved by the Institutional Animal Care and Use Committee of the University of Pennsylvania (IACUC-UPENN).

CEST imaging and ^{1}H MRS of the tissue were performed on a whole-body clinical 3-T Siemens Trio-Magnetom scanner (Malvern, PA, USA). CEST imaging of the normal lamb tissue was performed at 37 °C, whereas CEST imaging of the infarcted tissue was performed at only 25 °C to avoid potential autodegradation at 37 °C. We used a custom-designed Styrofoam chamber to maintain the temperature at 37 ± 1 °C. The pulse sequence used has been described previously[26]. A special optimized saturation pulse train was used with five Hanning-windowed rectangular pulses of 49-ms duration each with a 1-ms delay between them. The total repetition time was 10 s. The other parameters were as follows: slice thickness, 8 mm; GRE flip angle, 10°; readout repetition time (TR), 6.2 ms; echo time (TE), 3 ms; field-of-view, 100 × 100 mm^2; and image matrix size, 128 × 128. CEST images were collected using a saturation pulse B_{1rms} of 155 Hz (3.6 μT) and 250-ms duration. Single-voxel ^{1}H MRS spectra were obtained from the normal lamb tissue using a standard point-resolved spectroscopy[40] with the following parameters: voxel size, 8 × 8 × 8 mm^3; spectral width, 4 kHz; number of points, 2048; number of averages, 128; TE, 20 ms; and TR, 3 s. Water suppression was achieved using the variable pulse power and optimized relaxation delays method (VAPOR). The Cr peak was fitted to a Gaussian function using nonlinear least-squares fitting (MATLAB ‘nlinfit’ routine). Peak integrals were calculated and normalized with non–water suppressed proton signal for calculating Cr concentrations in *ex vivo* tissue.

In vivo animal imaging

Animal preparation and handling is described in Supplementary Methods. All animal studies were performed under a protocol approved by IACUC-UPENN for *in vivo* studies. Three male Yorkshire swine and two male Dorset sheep (Animal Biotech Industry, Doylestown, PA) weighing between 35 and 40 kg were used in this study. Animals were imaged with Siemens 3T clinical imaging system equipped with 40 mT/m nominal gradients, an 18-channel spine-array receive coil and a whole-body birdcage coil for transmission. CrEST imaging was performed with the application of the same imaging protocol as described for the *ex vivo* tissue, except field of view was adjusted on the basis of the animal size and the scans were gated to the electrocardiograph. The other parameters were a T_1 delay of 3 s and a segment number of 8. In-plane resolution was maintained at 1.5 × 1.5 mm^2. Z spectra were collected over a range of –6 to 6 p.p.m. with step size of 0.25 p.p.m. The scan time of the entire CrEST scan was ~45 min. Using the above imaging parameters, the power deposition

is well under the allowed limits of specific absorption rate. A typical example of pulse sequence is given in Supplementary Methods.

Chemical exchange saturation transfer and ^{31}P magnetic resonance spectroscopy in skeletal muscle

All human MR imaging and spectroscopy studies were performed on healthy volunteers in accordance with a protocol approved by the Institutional Review Board of the University of Pennsylvania. Written informed consent was obtained from all human subjects before MRI. CrEST imaging experiments on healthy human calf muscle (n = 3) were performed using an 8-channel ^{1}H knee coil on a 3-T whole-body scanner. Baseline imaging of human subjects was performed for 2 min, followed by 2 min of mild plantar flexion exercise and 8 min of post-exercise imaging. Plantar flexion exercise was performed using an MR-compatible, pneumatically controlled foot pedal. The pressure applied to the pedal was held constant at 8.5 psi across all the subjects. CrEST images were acquired for healthy volunteers using an optimized saturation pulse of 500 ms and a B_{1rms} of 93 Hz (2.25 μT) and imaging parameters as follows: slice thickness, 8 mm; flip angle, 10°; TR, 5.6 ms; TE, 2.7 ms; field of view, 140 × 140 mm^2; matrix size, 128 × 128; and T_1 delay, 4 s. Total imaging time for each CrEST map was 24 s.

Under identical experimental conditions and exercise levels, ^{31}P MRS was performed with a 7-cm-diameter ^{1}H-^{31}P dual-tuned surface coil using a unlocalized free induction decay sequence with the following parameters: number of points, 512; averages, 5; and TR, 2.4 s.

Image and spectroscopy processing details are provided in the Supplementary Methods.

Statistical analyses

Linear regression was performed to assess correlation among CrEST, ^{1}HMRS-derived concentration and Cr concentration measured from PCA analysis. For *in vivo* animals and human volunteer studies, the measured CrEST is reported as mean ± s.d.

Supplementary Material

Refer to Web version on PubMed Central for supplementary material.

Acknowledgments

This work was supported by National Institutes of Health grants P41 EB015893, P41 EB015893S1 and R21DA032256-01 and a pilot grant from the Translational Biomedical Imaging Center of the Institute for Translational Medicine and Therapeutics of the University of Pennsylvania. The authors acknowledge W. Liu and S. Pickup for technical assistance in using the 9.4-T NMR spectrometer, K. Nath for assistance with biochemical analysis and D. Reddy for help with regulatory protocol.

References

1. Balaban RS, Chesnick S, Hedges K, Samaha F, Heineman FW. Magnetization transfer contrast in MR imaging of the heart. Radiology. 1991; 180:671–675. [PubMed: 1871277]
2. Bax JJ, de Roos A, van Der Wall EE. Assessment of myocardial viability by MRI. J. Magn. Reson. Imaging. 1999; 10:418–422. [PubMed: 10508304]

3. Kim HW, Farzaneh-Far A, Kim RJ. Cardiovascular magnetic resonance in patients with myocardial infarction: current and emerging applications. J. Am. Coll. Cardiol. 2009; 55:1–16. [PubMed: 20117357]
4. Beek AM, et al. Delayed contrast-enhanced magnetic resonance imaging for the prediction of regional functional improvement after acute myocardial infarction. J. Am. Coll. Cardiol. 2003; 42:895–901. [PubMed: 12957439]
5. Schwitter J, Arai AE. Assessment of cardiac ischaemia and viability: role of cardiovascular magnetic resonance. Eur. Heart J. 2011; 32:799–809. [PubMed: 21398645]
6. Kim RJ, et al. The use of contrast-enhanced magnetic resonance imaging to identify reversible myocardial dysfunction. N. Engl. J. Med. 2000; 343:1445–1453. [PubMed: 11078769]
7. Bax JJ, et al. Metabolic imaging using F18-fluorodeoxyglucose to assess myocardial viability. Int. J. Card. Imaging. 1997; 13:145–155. discussion 157–160. [PubMed: 9110194]
8. Kitagawa K, et al. Acute myocardial infarction: myocardial viability assessment in patients early thereafter comparison of contrast-enhanced MR imaging with resting 201Tl SPECT. Single photon emission computed tomography. Radiology. 2003; 226:138–144. [PubMed: 12511682]
9. Bonow RO, Dilsizian V. Thallium 201 for assessment of myocardial viability. Semin. Nucl. Med. 1991; 21:230–241. [PubMed: 1948113]
10. Bax JJ, Van der Wall EE. Assessment of myocardial viability: guide to prognosis and clinical management. Eur. Heart J. 2000; 21:961–963. [PubMed: 10901505]
11. Crane P, Laliberte R, Heminway S, Thoolen M, Orlandi C. Effect of mitochondrial viability and metabolism on technetium-99m-sestamibi myocardial retention. Eur. J. Nucl. Med. 1993; 20:20–25. [PubMed: 7678396]
12. Dzeja PP, Redfield MM, Burnett JC, Terzic A. Failing energetics in failing hearts. Curr. Cardiol. Rep. 2000; 2:212–217. [PubMed: 10980895]
13. Reimer KA, Jennings RB, Tatum AH. Pathobiology of acute myocardial ischemia: metabolic, functional and ultrastructural studies. Am. J. Cardiol. 1983; 52:72A–81A.
14. Bottomley PA, Weiss RG. Non-invasive magnetic-resonance detection of creatine depletion in non-viable infarcted myocardium. Lancet. 1998; 351:714–718. [PubMed: 9504516]
15. Beer M, et al. Absolute concentrations of high-energy phosphate metabolites in normal, hypertrophied, and failing human myocardium measured noninvasively with 31P-SLOOP magnetic resonance spectroscopy. J. Am. Coll. Cardiol. 2002; 40:1267–1274. [PubMed: 12383574]
16. Neubauer S, et al. Absolute quantification of high energy phosphate metabolites in normal, hypertrophied and failing human myocardium. MAGMA. 2000; 11:73–74. [PubMed: 11186995]
17. Nakae I, et al. Proton magnetic resonance spectroscopy can detect creatine depletion associated with the progression of heart failure in cardiomyopathy. J. Am. Coll. Cardiol. 2003; 42:1587–1593. [PubMed: 14607443]
18. Metzler B, et al. Decreased high-energy phosphate ratios in the myocardium of men with diabetes mellitus type I. J. Cardiovasc. Magn. Reson. 2002; 4:493–502. [PubMed: 12549236]
19. Bottomley PA, Atalar E, Weiss RG. Human cardiac high-energy phosphate metabolite concentrations by 1D-resolved NMR spectroscopy. Magn. Reson. Med. 1996; 35:664–670. [PubMed: 8722817]
20. Hu Q, et al. Profound bioenergetic abnormalities in peri-infarct myocardial regions. Am. J. Physiol. Heart Circ. Physiol. 2006; 291:H648–H657. [PubMed: 16582014]
21. Zhou J, Payen JF, Wilson DA, Traystman RJ, van Zijl PC. Using the amide proton signals of intracellular proteins and peptides to detect pH effects in MRI. Nat. Med. 2003; 9:1085–1090. [PubMed: 12872167]
22. van Zijl PC, Jones CK, Ren J, Malloy CR, Sherry AD. MRI detection of glycogen in vivo by using chemical exchange saturation transfer imaging (glycoCEST). Proc. Natl. Acad. Sci. USA. 2007; 104:4359–4364. [PubMed: 17360529]
23. Ling W, Regatte RR, Navon G, Jerschow A. Assessment of glycosaminoglycan concentration in vivo by chemical exchange-dependent saturation transfer (gagCEST). Proc. Natl. Acad. Sci. USA. 2008; 105:2266–2270. [PubMed: 18268341]

24. Gilad AA, et al. Artificial reporter gene providing MRI contrast based on proton exchange. Nat. Biotechnol. 2007; 25:217–219. [PubMed: 17259977]
25. Haris M, Cai K, Singh A, Hariharan H, Reddy R. In vivo mapping of brain myo-inositol. Neuroimage. 2011; 54:2079–2085. [PubMed: 20951217]
26. Cai K, et al. Magnetic resonance imaging of glutamate. Nat. Med. 2012; 18:302–306. [PubMed: 22270722]
27. Haris M, et al. Exchange rates of creatine kinase metabolites: feasibility of imaging creatine by chemical exchange saturation transfer MRI. NMR Biomed. 2012; 25:1305–1309. [PubMed: 22431193]
28. Arús C, Barany M, Westler WM, Markley JL. 1H NMR of intact muscle at 11. T. FEBS Lett. 1984; 165:231–237.
29. Reijenga JC. Comparison of methanol and perchloric acid extraction procedures for analysis of nucleotides by isotachophoresis. J. Chromatogr. A. 1986; 374:162–169.
30. Woo D-C, et al. Regional absolute quantification of the neurochemical profile of the canine brain: investigation by proton nuclear magnetic resonance spectroscopy and tissue extraction. Appl. Magn. Reson. 2010; 38:65–74.
31. Bottomley PA, Weiss RG. Noninvasive localized MR quantification of creatine kinase metabolites in normal and infarcted canine myocardium. Radiology. 2001; 219:411–418. [PubMed: 11323465]
32. Liu G, Gilad AA, Bulte JW, van Zijl PC, McMahon MT. High-throughput screening of chemical exchange saturation transfer MR contrast agents. Contrast Media Mol. Imaging. 2010; 5:162–170. [PubMed: 20586030]
33. Laser A, et al. Regional biochemical remodeling in non-infarcted tissue of rat heart post-myocardial infarction. J. Mol. Cell. Cardiol. 1996; 28:1531–1538. [PubMed: 8841940]
34. Bottomley PA, Lee Y, Weiss RG. Total creatine in muscle: imaging and quantification with proton MR spectroscopy. Radiology. 1997; 204:403–410. [PubMed: 9240527]
35. Francescato MP, Cettolo V, di Prampero PE. Influence of phosphagen concentration on phosphocreatine breakdown kinetics. Data from human gastrocnemius muscle. J. Appl. Physiol. 2008; 105:158–164. [PubMed: 18436701]
36. van Vaals JJ, et al. “Keyhole” method for accelerating imaging of contrast agent uptake. J. Magn. Reson. Imaging. 1993; 3:671–675. [PubMed: 8347963]
37. Song HK, Dougherty L. k-space weighted image contrast (KWIC) for contrast manipulation in projection reconstruction MRI. Magn. Reson. Med. 2000; 44:825–832. [PubMed: 11108618]
38. Schroeder MA, et al. Hyperpolarized magnetic resonance: a novel technique for the in vivo assessment of cardiovascular disease. Circulation. 2011; 124:1580–1594. [PubMed: 21969318]
39. Lamb HJ, et al. Metabolic response of normal human myocardium to high-dose atropine-dobutamine stress studied by 31P-MRS. Circulation. 1997; 96:2969–2977. [PubMed: 9386164]
40. Bottomley PA. Spatial localization in NMR spectroscopy *in vivo*. Ann. NY Acad. Sci. 1987; 508:333–348. [PubMed: 3326459]

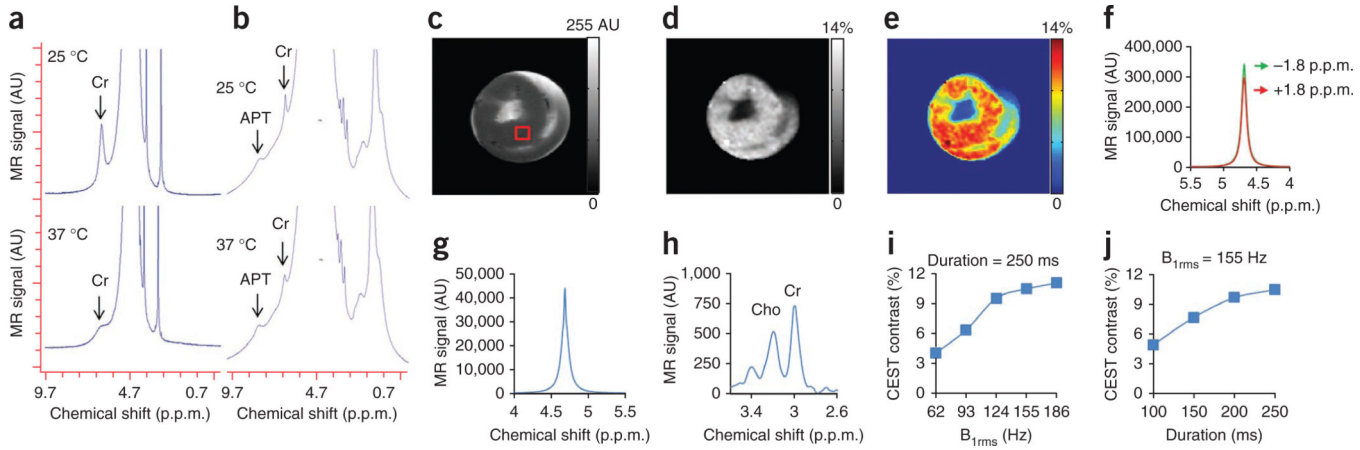

Figure 1.

CrEST measurement in *ex vivo* noninfarcted myocardial tissue. (**a,b**) Non–water-suppressed ^{1}H nuclear magnetic resonance (NMR) spectra from 100 mM creatine solution (reproduced from ref. 27) (**a**) and *ex vivo* myocardial tissue (**b**) obtained at two different temperatures (25 °C and 37 °C). The broad resonance at ~8.2 p.p.m. (~3.5 p.p.m. downfield of the bulk water) depicts the amide proton resonance from proteins. (**c**–**e**) The anatomical CEST-weighted image (2 p.p.m.) (**c**) and gray (**d**) and color-coded (**e**) CrEST maps of *ex vivo* myocardial tissue are shown. (**f**) Water spectra obtained from the tissue shown with saturation at ±1.8 p.p.m. using the B_{1rms} of 155 Hz (3.6 μT) and 250 ms. (**g,h**) The ratio of the integral of difference water spectrum (**g**) to the integral of Cr-CH_3 resonance from the same voxel from the water-suppressed spectra (**h**) is >70. AU, arbitrary units; Cho, choline methyl resonance. (**i,j**) Saturation pulse amplitude and duration dependence of CrEST are shown. The scale bars shown for anatomical images are MR image intensities in AU and the scale bars for all CrEST maps are CrEST contrasts in % units.

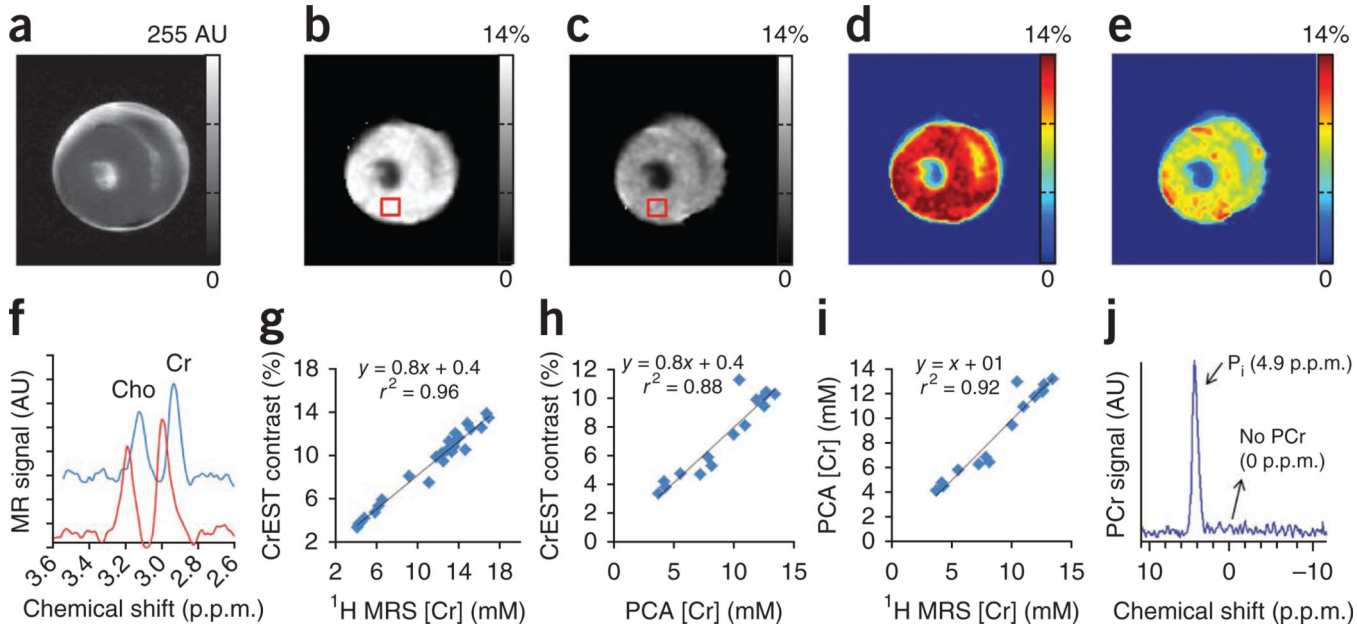

Figure 2.

CrEST map of a noninfarcted *ex vivo* lamb myocardium measured at two separate time points (14 h and 62 h) following excision of the heart. (**a**–**e**) Anatomical CEST-weighted image at 2 p.p.m. (**a**) and gray (**b** and **c**) and color-coded CrEST maps (**d** and **e**) are shown. The square boxes show the representative ROIs from where the water-suppressed ^{1}H MRS was measured. (**f**) ^{1}H MRS from the ROIs shown in **b** and **c**. Clear change in the Cr resonance amplitude measured at two different time points is evident. (**g**) Plot showing a linear correlation between Cr concentration and CrEST contrast (%). The *ex vivo* myocardial tissue exhibits 0.8% CrEST contrast per 1 mM Cr. (**h,i**) Correlations of Cr concentration, measured through PCA extraction, with both CrEST contrast (**h**) and ^{1}H MRS–measured Cr concentration (**i**) are shown. (**j**) On ^{31}P MRS of *ex vivo* myocardium, only P_i resonance is visible. The scale bars shown for anatomical images are MR image intensities in AU and the scale bars for all CrEST maps are CrEST contrasts in % units.

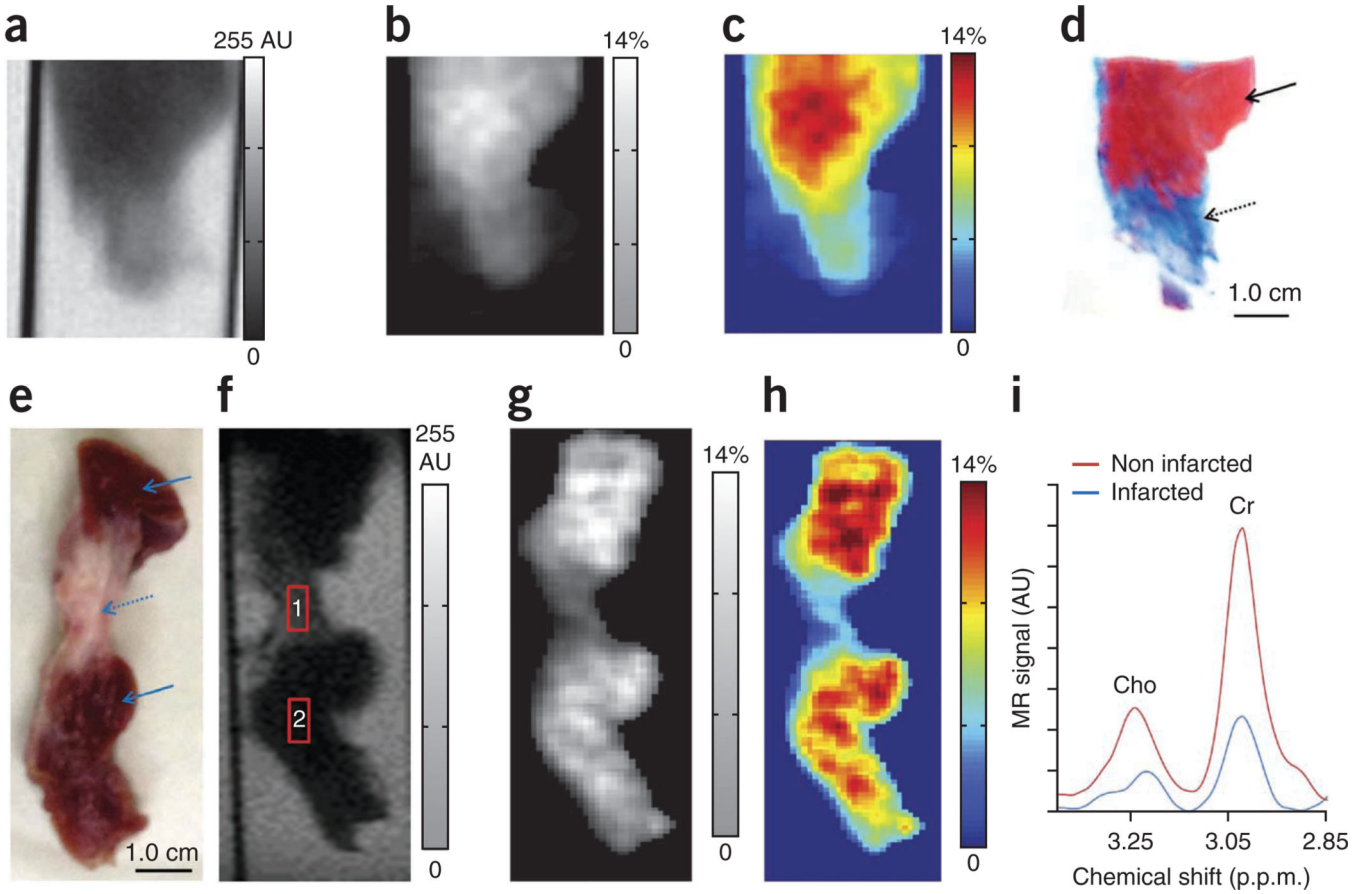

Figure 3.

Ex vivo CrEST of noninfarcted and infarcted myocardial tissue from swine. (**a**) Anatomical CEST-weighted image (2 p.p.m.) of an *ex vivo* myocardium tissue. (**b,c**) The CrEST contrast (%) shown in noninfarcted and infarcted regions in gray (**b**) and color-coded (**c**) CEST maps. (**d**) The trichrome stain of same tissue shows the infarcted region as blue (dotted arrow) and the noninfarcted region as red (solid arrow). The CrEST from the remote region is ~10.4%, whereas from the infarcted region it is ~4.7%. (**e**) Digital photograph of another myocardial tissue clearly depicts the infarcted (dotted arrow) and noninfarcted regions (solid arrow). (**f**) Anatomical CEST-weighted image (2 p.p.m.) of the tissue from **e** with the voxels placed on infarcted (1) and noninfarcted regions (2). (**g**–**i**) Grayscale (**g**) and color-coded (**h**) CrEST maps show CrEST contrast in noninfarcted and infarcted regions, and ^{1}HMRS (**i**) shows Cr resonance in noninfarcted and infarcted regions. The scale bars shown for anatomical images are MR image intensities in AU and the scale bars for all CrEST maps are CrEST contrasts in % units.

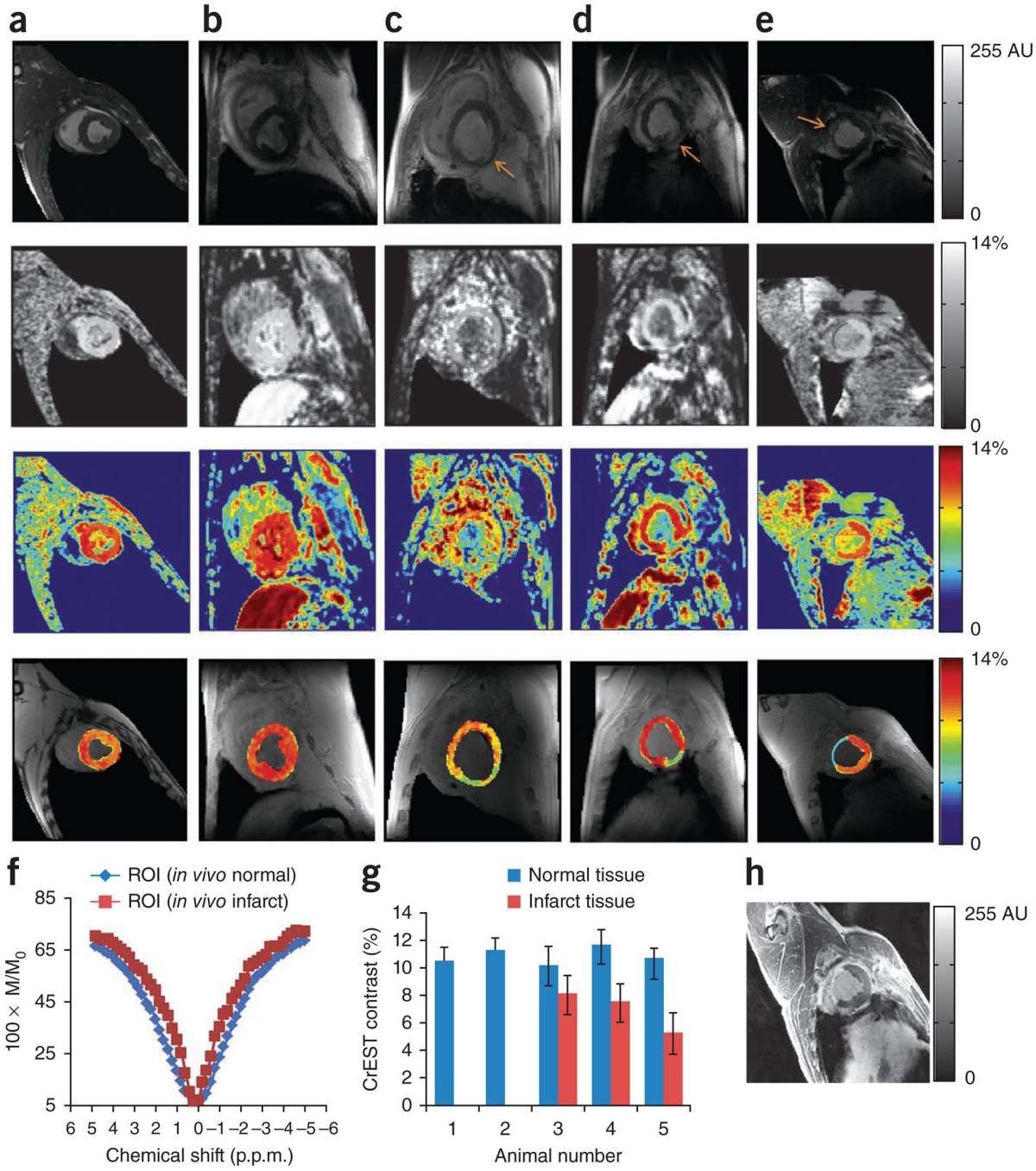

Figure 4.

In vivo CrEST data from normal and infarcted swine or sheep myocardium. (**a**–**e**) CrEST mapping of myocardium of two normal animals (swine, **a,b**) and three infarcted animals including two sheep (**c,d**) and one swine (**e**). The four rows show, from top to bottom, the anatomical CEST-weighted (2 p.p.m.) short-axis images of left ventricle, grayscale CrEST maps, color-coded CrEST maps and overlaid color-coded CrEST maps from all five animals. **c** and **d** show a 1-week infarction and **e** shows an 8-week infarction (arrows show the infarcted regions of the tissue). The process of identifying the wall is described in

Supplementary Methods. (**f**) The fitted *Z* spectra from normal and infarcted regions are shown (M and M_0 are water signal intensities with and without saturation, respectively). (**g**) Bar graph showing the CrEST contrast values in normal and infarcted regions of myocardium tissue. Data are expressed as mean ± s.d. (**h**) Delayed gadolinium-enhanced image of the 8-week infarcted swine myocardium, which shows hyperintensity in the infarcted region. The scale bars shown for anatomical images are MR image intensities in AU and the scale bars for all CrEST maps are CrEST contrasts in % units.

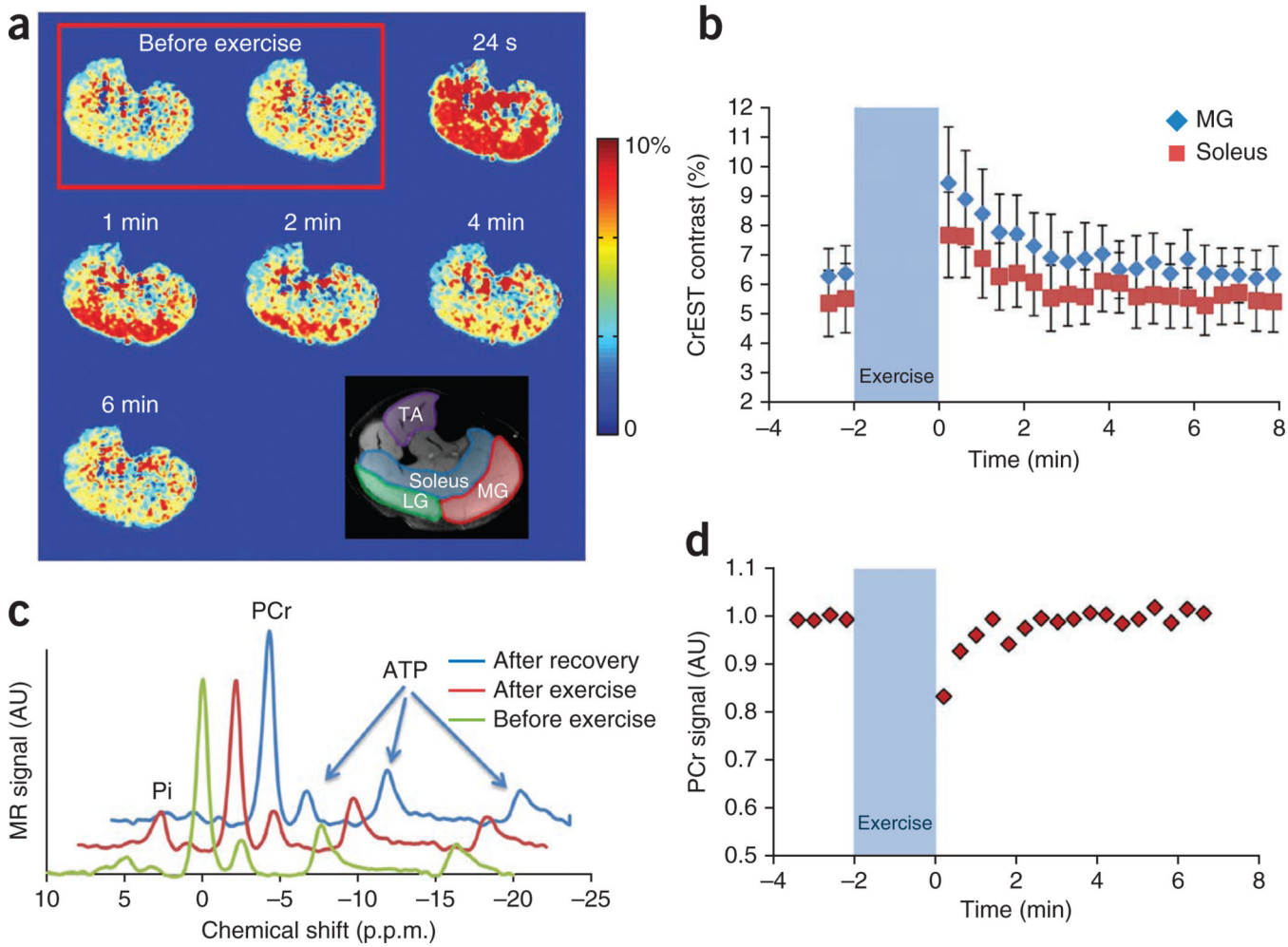

Figure 5.

CrEST maps of exercise-induced changes in skeletal muscle. (**a**) CrEST maps of healthy human calf before and after exercise, at different time points, show an increase in CrEST contrast immediately after exercise that corresponds to an increase in Cr concentration, followed by a return to the basal value CrEST contrast. Anatomic image of calf muscle overlaid with muscle groups highlighted is shown on the bottom right. (**b**) Kinetics of CrEST changes in different muscle groups depict post-exercise increases in CrEST contrast percentage and recovery to baseline levels. Data are expressed as mean ± s.d. (**c**) Representative ^{31}P MRS before exercise, immediately after exercise and after full recovery from exercise. The decrease in the PCr peak and increase in P_i peak immediately after exercise is shown. (**d**) PCr kinetics obtained from nonlocalized ^{31}P MRS from the same muscle region, showing a decrease in PCr signal immediately following exercise, which recovers back to baseline values. The scale bars shown for anatomical images are MR image intensities in AU and the scale bars for all CrEST maps are CrEST contrasts in % units.